Numerical Modeling of a Newtonian and Non-Newtonian Fluid Flow in Tubular Membranes Applied to the Microfiltration and Ultrafiltration Processes

Juliana Maria da Silva
School of Engineering, Department of Mechanical Engineering, University of São Paulo – São Calos/S.P.
jmaria02 @yahoo.com.br

Sérgio R. Fontes
School of Engineering, Department of Mechanical Engineering, University of São Paulo – São Calos/S.P.
srf @sc.usp.br

Abstract. *In this work, a laminar flow of a Newtonian and a non-Newtonian aqueous solution in a tubular membrane is studied numerically. The mathematical model comprises the conservation of mass, conservation of momentum and mass transfer equations in cylindrical coordinates with the associated boundary conditions. The suction velocity is described by Darcy's law (resistance-in-series model), that relates the permeate flux with the transmembrane pressure. The governing equations are solved numerically by a finite-difference method called SOLA on a staggered grid. Values to permeate flux are compared with experimental results of literature obtained from commercial membranes in different transmembrane pressure values.*

Keywords: Crossflow; *Porous tube; Modeling; Laminar; Non-Newtonian*

1. Introduction

The importance of Newtonian and non-Newtonian fluids in industrial processes, such as in the processing of emultions, pulpy fruits, suspensions, etc., has increased the interest in understanding the behavior of the flow of these fluids, especially the fluid flow through a tubular membrane, which is associated with industrial process called crossflow filtration. In this process, the solvent is forced to flow through the membrane by applying a transversal pressure (transmembrane pressure) across the permeable membrane. During the crossflow filtration, particles in the feed stream are brought to the membrane surface by convective transport and a portion of the solvent is removed from the fluid. The particles accumulate near the membrane surface until the equilibrium between convective e diffusive fluxes is reached. This process is illustrated in the Fig. 1.

The fraction of solute maintained near the membrane surface is called concentration polarisation. The major problem during membrane crossflow filtration is the permeate flux decline caused by concentration polarisation. In order to understand this process, several authors have studied the transport phenomena at the membrane surface.

Lee and Clark (1998) developed a numerical model to predict the permeate flux decline due to cake formation (concentration polarisation) during crossflow ultrafiltration of colloidal suspensions. Yeh (2002), Yeh et al. (2003) e Yeh et al. (2004) analysed the decline of permeate flux by taking the mass and momentum balances together with the consideration of flux loss and coupled with a resistance-in-series model. Damak et al. (2004) developed a numerical technique to solve the convective diffusion equation for particle transport in laminar flow over a permeable surface in a tubular membrane and investigated the effect of various physical parameters on the concentration. Other authors (Kumar, 1999; Kotzev, 1994; Geraldes, 2001) also worked with the formulation of the mass transfer to model the decline of permeate flux.

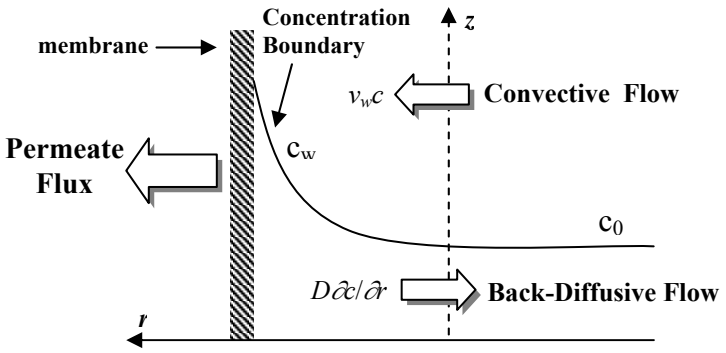

Figure 1. Scheme of concentration polarisation phenomenon during crossflow filtration.

Then, considering the interest in numerical solutions of models of flows in tubular membranes, the objectives of the present paper are to study numerically the flow of Newtonian and non-Newtonian aqueous solution in a tubular membrane and investigate the effects of several physical parameters on the concentration profile. For this, the mass conservation, momentum conservation and mass transport equations are discretized and implemented by the finite-difference technique, based on staggered grids. In this modeling the resistence-in-series model (Zeman and Zydney, 1996) is used to determine the local wall permeation velocity. The results are presented and compared with results of the literature.

2. Mathematical modeling of crossflow filtration

2.1. Mathematics formulation

Consider a laminar, isothermal, incompressible, axisymmetric and undeveloped flow in a circular tube with permeable walls. Because of symmetry, only the region between the wall ($r = R$) and centerline ($r = 0$) need to be considered. The geometry is shown in Fig. 2, where the cylindrical coordinate system has origin at the entrance, the z-axis is on the centerline, the r-axis is normal to the centerline, the inner radius and length of the tube are R and L, respectively.

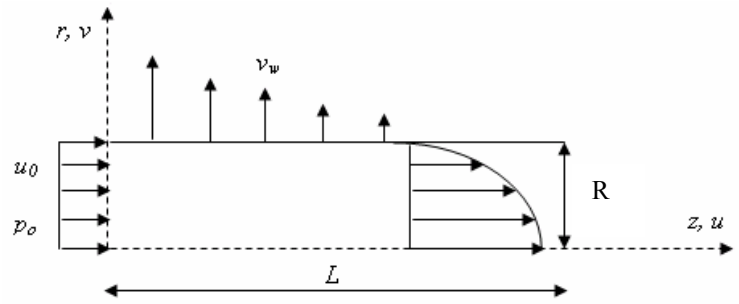

Figure 2. Representation of laminar flow in a tubular membrane.

Although the mass transfer reaches a steady-state in a very short period for a given velocity field, this work uses a transient model in order to observe the permeate flux decline during the cake formation. Then, in this work the crossflow filtration processes is described by mass conservation, momentum conservation (generalized to non-Newtonian fluid) and mass transport equations, which are expressed as follows:

Mass conservation:

$$\nabla \cdot \boldsymbol{u} = 0 \tag{1}$$

Momentum conservation:

$$\rho \frac{D}{Dt} \boldsymbol{u} = \nabla \cdot \sigma \tag{2}$$

where $\boldsymbol{u} = (u, v)$, σ e ρ are respectively, the fluid velocity, the stress tensor and the density. The constitutive equations for this problem are given by:

$$\sigma = -p\mathbf{I} + \tau, \qquad \tau = 2\eta(\dot{\gamma})\dot{\bar{\gamma}}, \qquad \dot{\bar{\gamma}} = \frac{1}{2}(\nabla \boldsymbol{u} + (\nabla \boldsymbol{u})^{\mathrm{T}}), \qquad \dot{\gamma} = \sqrt{2tr(\dot{\bar{\gamma}})} \tag{3}$$

where p is the fluid pressure, $\boldsymbol{I}$ is the identity tensor, τ is the extra-stress tensor, $\dot{\bar{\gamma}}$ is the rate-of-deformation tensor, $\dot{\gamma}$ is the local shear rate and $\eta(\dot{\gamma})$ is the apparent viscosity, which is defined by the power-law model (Bird et al., 1987):

$$\eta = m\dot{\gamma}^{n-1} \tag{4}$$

where m is the consistency index (with unit $Pa\ s^n$) and n (dimensionless) is the power-law index.

Mass transport:

$$\frac{\partial c}{\partial t}+\frac{\partial (uc)}{\partial z}+\frac{1}{r}\frac{\partial (rvc)}{\partial r}=D\left[\frac{\partial^2 c}{\partial r^2}+\frac{\partial^2 c}{\partial z^2}+\frac{1}{r}\frac{\partial c}{\partial r}\right] \tag{5}$$

where D (considered constant) is the diffusion coefficient.

2.2. Nondimensionalization

In this work, the mathematics formulation is put into the dimensionless form for the following variables:

$$\bar{z}=\frac{z}{R},\quad \bar{r}=\frac{r}{R},\quad \bar{u}=\frac{u}{u_0},\quad \bar{v}=\frac{v}{u_0},\quad \bar{p}=\frac{p}{\rho u_0^2},\quad \bar{t}=\frac{tu_0}{R},\quad \bar{c}=\frac{c}{c_0} \tag{6}$$

Then, with (3), (4) and (6) the equations (1), (2) and (5) can be cast in the forms:

$$\frac{\partial \bar{u}}{\partial \bar{z}}+\frac{1}{\bar{r}}\frac{\partial (\bar{r}\bar{v})}{\partial \bar{r}}=0 \tag{7}$$

$$\frac{\partial \bar{u}}{\partial \bar{t}}=-\frac{\partial \bar{p}}{\partial \bar{z}}+N_u \tag{8}$$

$$\frac{\partial \bar{v}}{\partial \bar{t}}=-\frac{\partial \bar{p}}{\partial \bar{r}}+N_v \tag{9}$$

$$\frac{\partial c}{\partial t}=-\frac{\partial (uc)}{\partial z}-\frac{1}{r}\frac{\partial (rvc)}{\partial r}+\frac{2}{Pe}\left[\frac{\partial^2 c}{\partial r^2}+\frac{\partial^2 c}{\partial z^2}+\frac{1}{r}\frac{\partial c}{\partial r}\right] \tag{10}$$

where

$$N_u=-\frac{\partial (\bar{u}\bar{u})}{\partial \bar{z}}-\frac{1}{\bar{r}}\frac{\partial (\bar{r}\bar{u}\bar{v})}{\partial \bar{r}}+\frac{2^n}{\mathrm{Re}}\left\{\frac{\partial}{\partial \bar{z}}\left(2\bar{\eta}\frac{\partial \bar{u}}{\partial \bar{z}}\right)+\frac{\bar{\eta}}{\bar{r}}\left(\frac{\partial \bar{u}}{\partial \bar{r}}+\frac{\partial \bar{v}}{\partial \bar{z}}\right)+\frac{\partial}{\partial \bar{r}}\left[\bar{\eta}\left(\frac{\partial \bar{u}}{\partial \bar{r}}+\frac{\partial \bar{v}}{\partial \bar{z}}\right)\right]\right\}$$

$$N_v=-\frac{\partial (\bar{u}\bar{v})}{\partial \bar{z}}-\frac{1}{\bar{r}}\frac{\partial (\bar{r}\bar{v}\bar{v})}{\partial \bar{r}}+\frac{2^n}{\mathrm{Re}}\left\{\frac{\partial}{\partial \bar{r}}\left(2\bar{\eta}\frac{\partial \bar{v}}{\partial \bar{r}}\right)+\frac{2\bar{\eta}}{\bar{r}}\frac{\partial \bar{v}}{\partial \bar{r}}-2\bar{\eta}\frac{\bar{v}}{\bar{r}^2}+\frac{\partial}{\partial \bar{z}}\left[\bar{\eta}\left(\frac{\partial \bar{u}}{\partial \bar{r}}+\frac{\partial \bar{v}}{\partial \bar{z}}\right)\right]\right\}$$

$$\bar{\eta}=\left\{2\left[\left(\frac{\partial \bar{u}}{\partial \bar{z}}\right)^2+\left(\frac{\partial \bar{v}}{\partial \bar{r}}\right)^2+\left(\frac{\bar{v}}{\bar{r}}\right)^2\right]+\left(\frac{\partial \bar{u}}{\partial \bar{r}}+\frac{\partial \bar{v}}{\partial \bar{z}}\right)^2\right\}^{\frac{n-1}{2}},\quad \mathrm{Re}=\frac{\rho u_0^{2-n}(2R)^n}{m},\quad Pe=\frac{u_0 2R}{D}$$

2.3. Boundary conditions

Dimensionless boundary conditions employed in the present study are given by:

$$\bar{z}=0,\qquad 0\le \bar{r}\le 1,\qquad \bar{u}=1,\qquad \bar{v}=0,\qquad \bar{c}=1 \tag{11}$$

$$\bar{z}=\frac{L}{R},\qquad 0\le \bar{r}\le 1,\qquad \frac{\partial \bar{u}}{\partial \bar{z}}=0,\quad \frac{\partial \bar{v}}{\partial \bar{z}}=0,\quad \frac{\partial \bar{c}}{\partial \bar{z}}=0 \tag{12}$$

$$\bar{r}=0,\qquad 0\le \bar{z}\le \frac{L}{R},\qquad \frac{\partial \bar{u}}{\partial \bar{r}}=0,\quad \vec{v}=0,\qquad \frac{\partial \bar{c}}{\partial \bar{r}}=0 \tag{13}$$

$$\bar{r}=1,\qquad 0\le \bar{z}\le \frac{L}{R},\qquad \bar{u}=0,\qquad \bar{v}=\bar{v}_w,\qquad \frac{Pe}{2}\vec{v}_w\bar{c}=\frac{\partial \bar{c}}{\partial \bar{r}} \tag{14}$$

where $\bar{v}_w$ is the local permeation velocity. The permeation velocity is given by the resistance-in-series model, defined by:

$$v_w = \frac{\Delta p}{R_m + R_p} \tag{15}$$

with R_m, R_p and Δp denoting the membrane resistance, the concentration polarisation layer resistance and transmembrane pressure, respectively. The resistances R_m and R_p are determined experimentally.

2.4. Numerical procedure

Equations (7)-(10) associated with the boundary conditions (11)-(14) are discretised by finite-difference scheme on a staggered grid, a typical cell of dimensions Δx by Δy. The variables: pressure p, concentration c and local shear rate $\dot{\gamma}$ are positioned at a cell centre, while u and v are staggered by translations of $\Delta x/2$ and $\Delta y/2$, respectively. The time derivatives are approximate by forward differences. The pressure derivates, the derivates of the mass conservation equation and the diffusive terms of the momentum and mass transport equations are approximate by central differences, while the convection terms are approximated by a second-order scheme, HLPA (hybrid linear/parabolic approximation) (Zhu, 1992). The pressure and velocity are solved by the SOLA method (Hirt et al., 1975; Fortuna, 2000). This method is characterized by the scheme of pressure and velocity corrections at each time step. The equations for correcting the pressure and velocity are written as follows:

$$\delta p_{i,j} = \frac{-\omega \nabla \cdot \bar{u}_{i,j}^{n+1}}{2\Delta\bar{t}\left(\frac{1}{(\Delta\bar{z})^2} + \frac{1}{(\Delta\bar{r})^2}\right)} \tag{16}$$

$$\bar{u}_{i+1/2,j}^{n+1} = \tilde{\bar{u}}_{i+1/2,j}^{n+1} + \Delta\bar{t}\,\frac{\delta\bar{p}_{i,j}}{\Delta\bar{z}}, \qquad \bar{u}_{i-1/2,j}^{n+1} = \tilde{\bar{u}}_{i-1/2,j}^{n+1} - \Delta\bar{t}\,\frac{\delta\bar{p}_{i,j}}{\Delta\bar{z}} \tag{17}$$

$$\bar{v}_{i,j+1/2}^{n+1} = \tilde{\bar{v}}_{i,j+1/2}^{n+1} + \Delta\bar{t}\,\frac{\delta\bar{p}_{i,j}}{\Delta\bar{r}}, \qquad \bar{v}_{i,j-1/2}^{n+1} = \tilde{\bar{v}}_{i,j-1/2}^{n+1} - \Delta\bar{t}\,\frac{\delta\bar{p}_{i,j}}{\Delta\bar{r}} \tag{18}$$

where ω is the relaxation factor, with $1 < \omega < 2$ and $\tilde{\bar{u}}_{i+1/2,j}^{n+1}$, $\tilde{\bar{u}}_{i-1/2,j}^{n+1}$, $\tilde{\bar{v}}_{i,j+1/2}^{n+1}$ and $\tilde{\bar{v}}_{i,j-1/2}^{n+1}$ are obtained from the discretization of the momentum equations:

$$\tilde{\bar{u}}_{i+1/2,j}^{(n+1)} = \bar{u}_{i+1/2,j}^{n} - \Delta\bar{t}\left(\frac{\bar{p}_{i+1,j}^{n} - \bar{p}_{i,j}^{n}}{\Delta\bar{z}} + N_{u_{i+1/2,j}}^{n}\right), \qquad \tilde{\bar{u}}_{i-1/2,j}^{(n+1)} = \bar{u}_{i-1/2,j}^{n} - \Delta\bar{t}\left(\frac{\bar{p}_{i,j}^{n} - \bar{p}_{i-1,j}^{n}}{\Delta\bar{z}} + N_{u_{i-1/2,j}}^{n}\right) \tag{19}$$

$$\tilde{\bar{v}}_{i,j+1/2}^{(n+1)} = \bar{v}_{i,j+1/2}^{n} - \Delta\bar{t}\left(\frac{\bar{p}_{i,j+1}^{n} - \bar{p}_{i,j}^{n}}{\Delta\bar{r}} + N_{v_{i,j+1/2}}^{n}\right), \qquad \tilde{\bar{v}}_{i,j-1/2}^{(n+1)} = \bar{v}_{i,j-1/2}^{n} - \Delta\bar{t}\left(\frac{\bar{p}_{i,j}^{n} - \bar{p}_{i,j-1}^{n}}{\Delta\bar{r}} + N_{v_{i,j-1/2}}^{n}\right) \tag{20}$$

where Δt is the time-step.

2.4.1 Stability condition

The explicity discretization of the governing equations imposes restriction on the time-step. At each cycle the time-step size is obtained from:
(i) No particles should cross more than one cell boundary in a given time-step (Tomé, 1996; Fortuna, 2000):

$$\Delta\bar{t} < \min\left(\frac{\Delta\bar{x}}{|\bar{u}|_{\max}}, \frac{\Delta\bar{y}}{|\bar{v}|_{\max}}\right) \tag{21}$$

where u_{max} and v_{max} are the maximum values of u and v, respectively,
(ii) The second stability restriction is due to the explicit discretization of the momemtum equation and involves the Reynolds number and the viscosity (Tomé, 1996):

$$\Delta\bar{t} < \frac{\mathrm{Re}}{2^{n+1}\bar{\eta}_{\max}} \frac{\Delta\bar{z}^2 \Delta\bar{r}^2}{\Delta\bar{x}^2 + \Delta\bar{r}^2} \tag{22}$$

where

$$\bar{\eta}_{\max} = \max\{\bar{\eta}_{i,j}\}$$

(iii) Analogous with the restriction (ii), the third stability restriction is due to the explicit discretization of the mass transport:

$$\Delta\bar{t} < \frac{Pe}{4} \frac{\Delta\bar{z}^2 \Delta\bar{r}^2}{\Delta\bar{x}^2 + \Delta\bar{r}^2} \tag{23}$$

3. Results and discussion

The model presented in this work was used in simulations of Newtonian and non-Newtonian fluids flow, in commercial tubular membrane with a 0.0063m inner diameter and of a length 30 times the radius.

Figure 3 and Fig. 4 show numerical results for two non-Newtonian fluids, which are aqueous solutions of guar gum and xanthan gum (Fontes, 2005) with power-law index (n) equal to 0.87 and 0.42, respectively. The Reynolds number is 100, feed concentration (c_0) 0.1wt.% (1000 ppm), membrane resistance (R_m) equal to 2.3×10^6 Pa s m^{-1} and concentration polarisation layer resistance (R_p) equal to 2×10^{10} Pa s m^{-1} for n equal to 0.87 and 9.43×10^9 Pa s m^{-1} for n equal to 0.42.

Figure 3 shows the graph of the average permeate flux as a function of the inlet transmembrane pressure. It can be observed that the average permeate flux increases as the inlet transmembrane pressure increases, this result is due to the resistance-in-series model (Eq. 15) in which the permeate flux increases with the transmembrane pressure for constant R_m and R_p. Because of the permeate flux increase more particles are expected to be convectively driven to the membrane surface, as shown in Fig. 4, which presents results of the variation of local concentration to various inlet transmembrane pressure. These numerical results are in agreement with the physical problem and experimental observation (Zeman and Zydney, 1996).

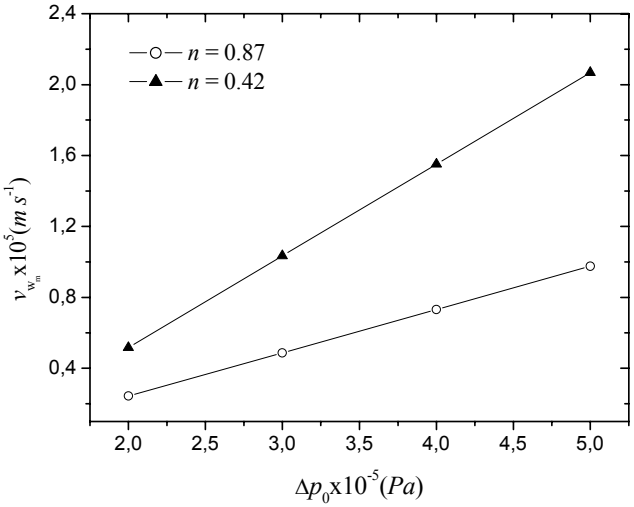

Figure 3. Numerical results of the two non-Newtonian fluids.

The average permeate flux is defined by the equation:

$$v_{w_m} = \frac{1}{L}\int_0^L v_w(z,R)dz \tag{24}$$

where the integral is calculated numerically by Trapezium formula using the finite difference scheme.

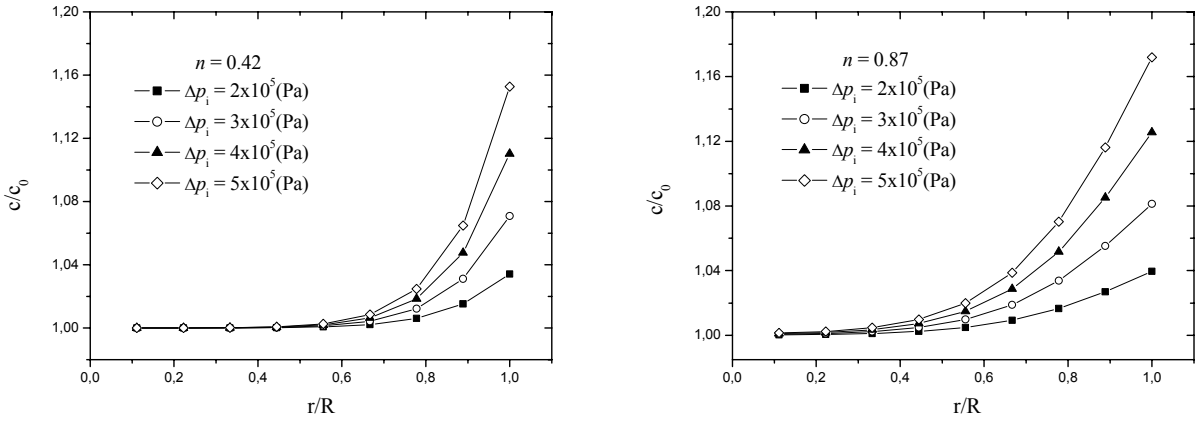

Figure 4. Local concentration as a function of the radial coordinate $\bar{r}$ at $\bar{z} = 1L/R$ for different inlet transmembrana pressure.

In order to validate the model, the numerical results are compared with some experimental values obtained from yeh et al. (2004) concerning the evolution of the average permeate flux as a function the inlet transmembrane pressure for a Dextran T500 solution, which is characterized by a power-law index equal to 1. It is observed in the Fig. 5 the good agreement of the numerical results with the experimental measurements. Two particular feed velocities were used, for $u_0 = 0.059 m\ s^{-1}$ there is good agreement in the results for the transmembrane pressure between $0.3\times10^5 Pa$ and $0.8\times10^5 Pa$, while to $u_0 = 0.147 m\ s^{-1}$ the agreement is adequate for the transmembrane pressure between $0.3\times10^5 Pa$ and $1.2\times10^5 Pa$.

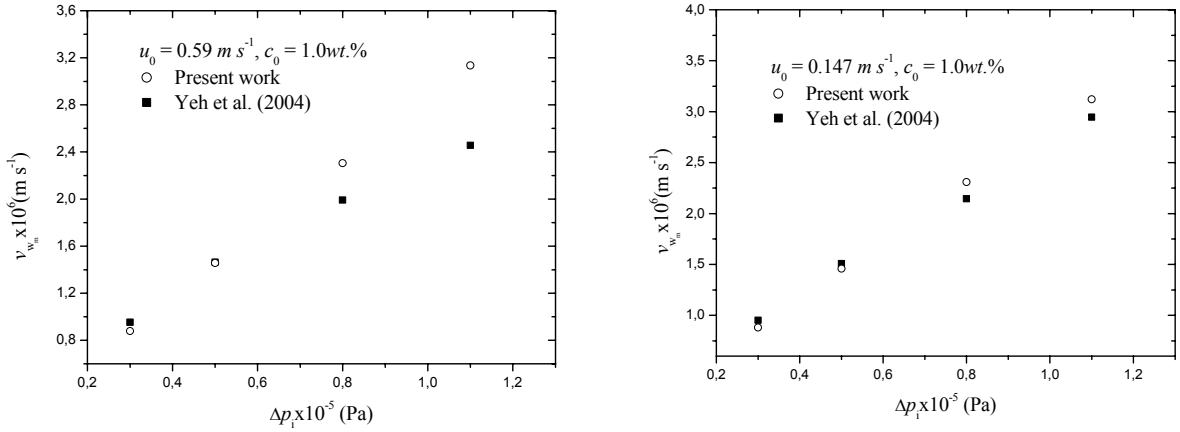

Figure 5. Comparison of numerical values with experimental values of the average permeate flux for a Dextran T500 solution.

Figure 6 represents the variation of dimensionless local concentration ($\bar{c}$) as a function of the radial coordinate ($\bar{r}$) at $\bar{z} = L/R$ for various axial Reynolds number in a hollow fiber membrane (Yeh et al., 2003). It is observed that concentration values on the membrane surface ($\bar{r}$ =1) increases as the Reynolds number decreases. This is a trend observed in the literature, as high axial Reynolds number (high axial velocity) impedes the accumulation of solutes on the membrane surface (Zeman and Zydney, 1996; Damak et al., 2004).

In general, after a small time interval (about 10 or 20 minutes) from the start of the process, the mass transfer reaches a quasi-steady-state, at this point, the particle deposition rate is in equilibrium with the particles diffusion rate, hence the permeate flux is in pseudo steady-state.

Figure 7 shows the model behavior in response to various feed concentrations of a Dextran T500 solution, which reaches the pseudo steady-state with rapidity (about 1 minute). As expected the simulations show that the permeate flux become smaller as the feed concentration increases, as the accumulation of solutes on the membrane surface increases with the feed concentration.

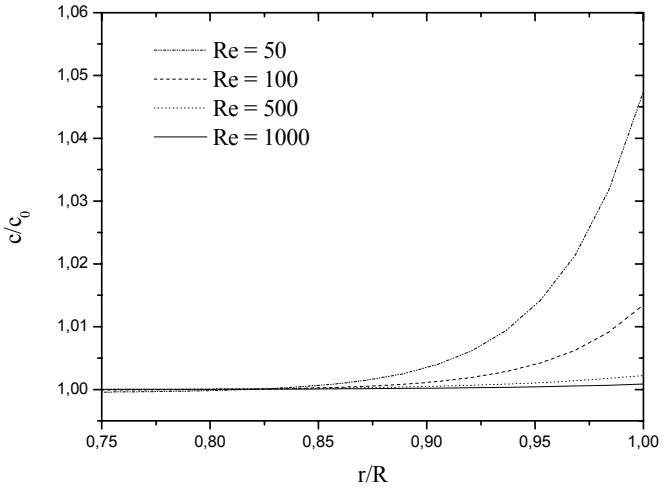

Figure 6. Plot of dimensionless concentration ($\bar{c}$) as a function of dimensionless radial location ($\bar{r}$) of a Dextran T500 solution for Reynolds number between 50 and 1000.

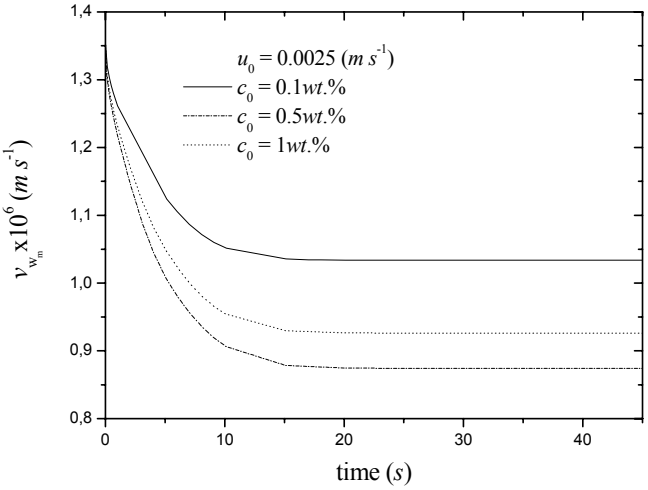

Figure 7. Average permeate flux as a function of time for different feed concentration.

4. Conclusions

The numerical results for the variation of the permeate flux of non-Newtonian fluids with power-law indexes 0.42 and 0.87 presented a qualitative behavior compatible with the literature. The model was tested for a Newtonian fluid (Dextran T500 solution) and presented good agreement with experimental results (Yeh et al., 2004). Therefore, the described model for the combination of the mass conservation, momentum conservation and mass transport equations with the resistance-in-series model, seems to be compatible with the phenomena associated to the studied physical problem (Zeman and Zydney, 1996).

5. Acknowledgements

The authors wish to express their thanks to the National Council of the Scientific and Technological Development (CNPq) for the financial support.

6. References

Bird, R.B., Armstrong, R.C. and Hassager, O., 1987, "Dynamics of Polymeric Liquids", Wesley Interscience, Vol. 1.

Damak, K., Ayadi, A., Schimitz, P. and Zeghmati, B., 2004, "Modeling of Crossflow Membrane Separation Processes under Laminar Flow Conditions in Tubular Membrane", Desalination, Vol. 168, pp. 231-239.

Fontes, S.R., 2005, "Mass Transfer in Microfiltration with Laminar and Turbulent Flow of Macromolecular Solutions", Journal of Membrane Science, Vol. 249, pp. 207-211.

Fortuna, A.O., 2000, "Técnicas Computacionais para Dinâmica dos Fluidos – Conceitos Básicos e Aplicações", Editora da Universidade de São Paulo.

Geraldes, V., semião, V. and Pinho, M.N., 2001, "Flow and Mass Transfer Modelling of Nanofiltration", Journal of Membrane Science, Vol. 191, pp. 109-128.

Hirt, C.W., Nichols, B.D. and Romero, N.C., 1975, "SOLA – A Numerical Solution Algorithm for Transiente Fluid Flows", Los Alamos Scientific Report LA-5852.

Kotzev, T., 1994, "Numerical Study of the Fluid Dynamics and Mass Transfer of na Ultrafiltration Performance in a Tube Membrane Module", International Journal of engineering Science, Vol. 32, pp. 359-368.

Kumar, V. and Upadhyay, S.N., 1999, "Computer Simulation of Membrane Processes: Ultrafiltration and Dialysis Units", Computers and Chemical Engineering, Vol. 23, pp. 1713-1724.

Lee, Y. and Clark, M.M., 1998, "Modeling of Flux Decline During Crossflow Ultrafiltration of Colloidal Suspensions", Journal of Membrane Science, Vol. 149, pp, 181-202.

Tomé, M.F., Duffy, B. and McKee, S., 1996, "A Numerical Technique for Solving Unsteady Non-Newtonian Free Surface Flows", Journal of Non-Newtonian Fluid Mechanics, Vol. 62, pp. 9-34.

Yeh, H.M., 2002, "Decline of Permeate Flux for Ultrafiltration Along Membrane Tubes", Desalination, Vol. 145, pp. 153-157.

Yeh, H.M., Wu, H.P., Dong, J.F., 2003, "Effects of design and operating parameters on the declination of permeate flux for membrane ultrafiltration along hollow-fiber modules", Vol. 213, pp 33-44.

Yeh, H.M., Dong, J.H. and Shi, M.Y., 2004, "Momemtum Balance Analysis of Flux and Pressure Declines in Membrane Ultrafiltration Along Tubular Modules", Vol. 241, pp. 335-345.

Zeman, L.J., Zydney, A.L.. Microfiltration and Ultrafiltration - Principles and Applications, Marcel Dekker, New York, 1996.

Zhu, J., 1992, "On the Higher-Order Bounded Discretization Schemes for Finite Volume Computations of Incompressible Flows", Computer in Applied Mechanics and Engineering, Vol. 98, pp. 345-360.

7. Responsibility notice

The authors are the only responsible for the printed material included in this paper.